Cholesterol metabolism in LUAD progression: GJB3 as a key target for cell-based therapeutic interventions

QIHANG YAN[1,2*], WUGUANG CHANG[3*], WINGSHING WONG[1,2*], LI GONG[1], DACHUAN LIANG[1], JIE YANG[1] and JUNYE WANG[1,2]

[1]State Key Laboratory of Oncology in South China, Guangdong Provincial Clinical Research Center for Cancer, Sun Yat-sen University Cancer Center, Guangzhou, Guangdong 510060, P.R. China; [2]Guangdong Esophageal Cancer Institute, Guangzhou, Guangdong 510060, P.R. China; [3]Guangdong Provincial Engineering Research Center of Molecular Imaging, The Fifth Affiliated Hospital of Sun Yat-sen University, Zhuhai, Guangdong 519000, P.R. China

Received February 18, 2025; Accepted August 5, 2025

DOI: 10.3892/mmr.2025.13694

Abstract. Cholesterol metabolism reprogramming serves a pivotal role in tumor onset and progression. The present study investigated lung adenocarcinoma (LUAD), focusing on the regulatory impact of cholesterol metabolism-related genes (CMRGs). Consensus clustering identified distinct cholesterol metabolism-related clusters in LUAD, followed by survival analysis and immune infiltration profiling for each cluster. A predictive model, constructed using cluster-specific differentially expressed genes and the LASSO algorithm, was validated with an independent dataset. Furthermore, the model was utilized to predict potential responses to immunotherapy and chemotherapy for patients with LUAD. The functional role of the key gene GJB3 in LUAD progression was confirmed through *in vitro* experiments. Two distinct cholesterol metabolism-related clusters were identified, exhibiting significant differences in prognosis, biological function and immune cell infiltration. A survival model, based on four genes, demonstrated strong predictive performance across multiple datasets. The low-risk group showed improved responses to immunotherapy, while the high-risk group exhibited heightened sensitivity to chemotherapy. *In vitro* assays revealed that GJB3 knockdown suppressed LUAD cell proliferation and invasion, significantly reducing the expression of epithelial-mesenchymal transition-related genes. These findings highlight CMRGs as potential prognostic biomarkers and suggest a foundation for personalized treatment strategies in LUAD.

Correspondence to: Dr Junye Wang, State Key Laboratory of Oncology in South China, Guangdong Provincial Clinical Research Center for Cancer, Sun Yat-sen University Cancer Center, 651 Dongfeng East Road, Guangzhou, Guangdong 510060, P.R. China
E-mail: wangjy@sysucc.org.cn

*Contributed equally

Key words: cholesterol metabolism, prognosis, lung adenocarcinoma, immunotherapy, GJB3

Introduction

Lung cancer remains a leading cause of global mortality (1), with tobacco use, occupational exposure and genetic factors being key contributors to its high incidence (2). Lung adenocarcinoma (LUAD) and lung squamous cell carcinoma are the two main subtypes of non-small-cell lung cancer (NSCLC) (3). Notably, with the advent of precision medicine, treatment strategies for LUAD have undergone transformative changes, incorporating targeted therapy and immunotherapy (4). However, genetic mutations, acquired resistance and epigenetic modifications inevitably lead to drug resistance in patients (5). Therefore, identifying novel therapeutic markers to more accurately characterize LUAD is crucial for overcoming treatment resistance.

Cancer cells, which exhibit uncontrolled proliferation, require elevated cholesterol levels for membrane synthesis and other vital functions (6), making cholesterol metabolism reprogramming a common feature in cancer. Dysregulation of proto-oncogenes and oncogenes results in notable increases in cholesterol uptake and the production of its derivatives within tumor cells (7,8). Additionally, the tumor microenvironment (TME), characterized by factors such as acidity and inflammation, further promotes cholesterol biosynthesis and uptake (9,10). 22-Hydroxycholesterol, a metabolite of cholesterol abundant in the TME (11), recruits neutrophils by binding to CXCR2, thereby exerting immunosuppressive effects (12). Tumor-associated macrophages also undergo functional and phenotypic alterations due to shifts in cholesterol metabolism, contributing to tumor progression (13). In summary, cholesterol and its metabolites drive tumor progression by enhancing tumor malignancy and remodeling the TME. Therefore, statin-based inhibition of active cholesterol metabolism has emerged as a promising antitumor strategy (14).

The aim of the present study was to identify potential biomarkers associated with cholesterol metabolism in the diagnosis of LUAD. The study aimed to screen differentially expressed genes related to cholesterol metabolism between LUAD and normal lung tissues, analyze their gene functions, and prognostic and clinical relevance, and perform cell

experiments to validate the functions of the selected genes. The current study established a robust diagnostic and prognostic model for patients with LUAD.

Materials and methods

Data collection and processing. RNA-sequencing data from patients with LUAD were obtained from The Cancer Genome Atlas (TCGA) database (https://portal.gdc.cancer.gov/), Subsequently, R project (v4.0.4; https://www.r-project.org/) was used for rigorous quality control and screening to remove duplicate samples, ensuring dataset uniqueness and reliability. Samples with a survival time of <30 days were excluded to ensure complete and usable survival data. A training set consisting of 485 LUAD samples and 59 paracancerous tissues was selected from TCGA, and a validation set (GSE72094) (15) was obtained from the Gene Expression Omnibus (https://www.ncbi.nlm.nih.gov/gds), comprising 398 samples with complete clinical data. cholesterol metabolism-related genes (CMRGs) were downloaded from MSigDB (https://www.gsea-msigdb.org/gsea/msigdb) (16), totaling 158 genes.

Consensus cluster analysis. Univariate Cox regression analysis was performed to assess the relationship between CMRGs and prognosis. TCGA cohort was clustered using the consensus clustering algorithm implemented through the 'ConsensusClusterPlus' R package (v3.0; https://bioconductor.org/packages/3.0/bioc/html/ConsensusClusterPlus.html) (17). Clustering was conducted with the PAM algorithm based on 1-Pearson correlation distance, with 80% of the samples repeated 1,000 times. The optimal number of clusters was determined through analysis of the empirical cumulative distribution function (CDF) plot. A Sankey diagram was generated using the 'ggplot2' R package (v 3.3.0; https://cran.r-project.org/web/packages/ggplot2/index.html).

Gene set enrichment analysis (GSEA). GSEA was performed using 'c5.go.v7.5.1.symbols' (Gene Ontology terms) and 'c2.cp.kegg.v7.5.1.symbols' (Kyoto Encyclopedia of Genes and Genomes) from the molecular signature database (https://www.gsea-msigdb.org/gsea/index.jsp) to explore biological signatures and pathways across different clusters (18).

TME analysis. Using the single sample GSEA algorithm, the activity levels of 28 immune cell types were evaluated for each sample (in the GSE72094 dataset) (19). The ESTIMATE algorithm, applied to pre-screened immune-related gene expression data, was used to predict cell infiltration and tumor purity in LUAD tissues (TCGA) (20).

Construction of cholesterol metabolism gene signature. Differentially expressed genes between clusters were identified using 'limma' R package (v3.42.2; http://bioconductor.org/packages/3.10/bioc/html/limma.html) analysis of variance (21), and genes with a P-value of <0.05 and fold change of ≥2 were further analyzed using univariate or LASSO Cox regression. The risk index for each patient was calculated by multiplying the expression levels of target genes by their corresponding coefficients. Based on the median risk index, patients with LUAD were categorized into high-risk and low-risk groups for subsequent analyses. Kaplan-Meier curves and log-rank tests were used to assess survival differences, with the same analysis applied to validate the prognostic model in the GSE72094 dataset.

Nomogram development and validation. Univariate and multivariate Cox regression analyses were conducted using R project to assess the independence of the risk index from traditional clinical features. A nomogram was created to visually represent the significant risk index (P<0.05) alongside other risk factors. Calibration curves and time-dependent receiver operating characteristic curves were generated to evaluate the prognostic predictive power of the nomogram at various time points.

Analysis of tumor mutation burden (TMB). Somatic mutation data for LUAD cases were sourced from TCGA database, with TMB calculated by quantifying somatic non-synonymous mutations within defined genomic regions. The 'maftools_2.24.0' R package (https://bioconductor.org/packages/release/bioc/vignettes/maftools/inst/doc/maftools.html) was used to analyze the correlation between risk scores and TMB using the Pearson correlation coefficient.

Prediction of immunotherapy and chemotherapy response. The response of solid tumors to treatment with immune checkpoint inhibitors (ICIs) was predicted using the Tumor Immune Dysfunction and Exclusion (TIDE) (http://tide.dfci.harvard.edu) algorithm, which evaluates immune cell infiltration and dysfunction levels (22). The TIDE score for each patient with LUAD (from TCGA dataset) was calculated based on their expression profile, with higher TIDE scores indicating an increased potential for ICI resistance. Additionally, the 'pRRophetic_0.5' R package (https://github.com/paulgeeleher/pRRophetic2) was employed to estimate the half maximal inhibitory concentration values for various chemotherapy agents in patients with LUAD (from TCGA dataset).

Cell culture. Two human LUAD cell lines, A549 and NCI-H1975, were purchased from Wuhan Pricella Biotechnology Co., Ltd. A549 cells were cultured in F12K medium (Gibco; Thermo Fisher Scientific, Inc.), while NCI-H1975 cells were cultured in RPMI-1640 medium (Gibco; Thermo Fisher Scientific, Inc.). All of the media were supplemented with 10% fetal bovine serum (NEWZERUM Ltd.) and 1% penicillin/streptomycin in a 5% CO_2 incubator at 37˚C. Small interfering (si)RNAs were synthesized by Guangzhou RiboBio Co., Ltd. with the following sequences and targets (5'-3'): Non-targeting siRNA-negative control, antisense strand: ACGUGACACGUUCGGAGAA, sense strand: CUCCGAACGUGUCUCGUAA; GJB3-siRNA1, antisense strand: AGACCUUGUACCCACAGCGGG, sense strand: CGCUGUGGGUACAAGGUCUGC (target: CCCGCUGUGGGUACAAGGUCUGC); GJB3-siRNA2, antisense strand: AGGACUCGCCCACGCUAGUUU, sense strand: ACUAGCGUGGGCGAGUCCUGA, (target: AAACUAGCGUGGGCGAGUCCUGA); GJB3-siRNA3, antisense strand: UGGCGCGGGACCUUGACCGUG, sense strand: CGGUCAAGGUCCCGCGCCAAG (target: CACGGUCAAGGUCCCGCGCCAAG). Transfection was performed using Lipofectamine®

RNAiMAX (Invitrogen; Thermo Fisher Scientific, Inc.), and A549 and NCI-H1975 cells were used for transfection. Briefly, when the cell confluence was 30-50%, Opti-MEM (Gibco; Thermo Fisher Scientific, Inc.), 10 nm siRNA and Lipofectamine RNAiMAX reagent were successively added to a sterile microcentrifuge tube, gently mixed and incubated for 20 min at room temperature (25˚C). After 20 min, the transfection complexes were successively added to the cell culture dishes, gently mixed and placed in the cell incubator for 6 h at 37˚C. Subsequent experiments were performed 48 h after transfection.

Western blotting. After transfection, the cells were lysed with RIPA buffer (Merck KGaA) containing protease inhibitors (Merck KGaA). Protein concentrations were determined using the BCA kit (Nanjing KeyGen Biotech Co., Ltd.), and proteins (30 μg/lane) were separated by SDS-PAGE on 10% gels. Following transfer to PVDF membranes (Merck KGaA), protein blocking was carried out with 5% skim milk at room temperature for 1 h. The membranes were then incubated with primary antibodies overnight at 4˚C, followed by secondary antibody incubation at room temperature for 1 h. Blots were detected using Ultra-sensitive ECL chemiluminescent substrate (cat. no. BL523B; Biosharp Life Sciences) and images were captured with a Tanon 5200 system (Tanon Science and Technology Co., Ltd.). The following antibodies were used for western blotting: GJB3 polyclonal antibody (cat. no. 12880-1-AP; Proteintech Group, Inc.), E-cadherin polyclonal antibody (cat. no. 20874-1-AP; Proteintech Group, Inc.), N-cadherin polyclonal antibody (cat. no. 22018-1-AP; Proteintech Group, Inc.), vimentin polyclonal antibody (cat. no. 10366-1-AP; Proteintech Group, Inc.), Snail1 polyclonal antibody (cat. no. 13099-1-AP; Proteintech Group, Inc.), β-actin recombinant antibody (cat. no. 81115-1-RR; Proteintech Group, Inc.) and Goat Anti-Rabbit IgG H&L antibody (cat. no. BF03008; Biodragon).

Cell viability and proliferation assays. Cell viability was evaluated using the Cell Counting Kit (CCK)-8 (Dojindo Laboratories, Inc.). Cells were seeded in 96-well plates at 1,000 cells/well and cultured in a 5% CO_2 incubator at 37˚C. After 6 h, the cells adhered to the surface of the plates, and measurements at this time were considered 0-h data. Subsequently, CCK-8 values were measured every 24 h, and the data at 0, 24, 48, 72, 96 and 120 h time points were analyzed and plotted. Cells were seeded in 96-well plates and cultured in a 5% CO_2 incubator at 37˚C. Subsequently, 100 μl complete medium containing 10% CCK-8 reagent was added to each well, and incubation was continued for 1 h. Absorbance at OD_{450} was measured using the MD SpectraMax Plus 384 (Molecular Devices, Inc.).

On day 5 of culture, cell proliferation was assessed using the Click-iT EdU-488 Cell Proliferation Detection Kit (Wuhan Servicebio Technology Co., Ltd.), with 1 μg/ml Hoechst 33342 and 10 μM EdU used for detection. EdU staining experiments were performed according to the manufacturer's protocol. Images were captured using a Nikon ECLIPSE Ti-2 fluorescence microscope (Nikon Corporation), with excitation/emission wavelengths of 346/460 nm for Hoechst and 491/516 nm for EdU.

Colony formation assay. For colony formation assays, cells were seeded in 6-well plates at 1,000 cells/well and cultured in a 5% CO_2 incubator at 37˚C, with the medium changed every 3 days. After 2 weeks, the cells were fixed in 4% paraformaldehyde at room temperature for 60 min and stained with 0.1% crystal violet (Beyotime Institute of Biotechnology) at room temperature for 5 min. The colonies were rinsed with tap water, dried and images were captured using a digital camera. The data were statistically analyzed according to the area of crystal violet staining.

Migration and invasion assays. Cell migration and invasion were assessed using 24-well Transwell Tissue Culture Plate Inserts (pore size, 8.0 μm) (Guangzhou Jet Bio-Filtration Co., Ltd.). For the migration assay, 2,000 cells/well were seeded in the upper chamber of an uncoated Transwell insert, whereas for the invasion assay, the upper chamber was coated with VitroGel™ 3D hydrogel (cat. no. VHM01; Shanghai XP Biomed Ltd.) at room temperature for 10-15 min. The cells were seeded in the upper chamber in serum-free medium, whereas the lower chamber contained complete medium; the cells were cultured in a 5% CO_2 incubator at 37˚C. After 24 h of incubation, the cells were fixed with 4% paraformaldehyde at room temperature for 60 min and stained with 0.1% crystal violet at room temperature for 5 min. After rinsing with tap water and drying, images were captured using Nikon ECLIPSE Ti-2 light microscope channel (Nikon Corporation).

Statistical analysis. Data analysis and image processing were performed using R software (version 4.1.3) (https://www.r-project.org/) and GraphPad Prism 9 (Dotmatics). Differences between continuous variables were analyzed using the Wilcoxon rank-sum test, while categorical variables were assessed using the χ^2 test. Survival analysis was conducted using the log-rank test. Spearman's rank correlation was applied for correlation analysis. $P<0.05$ was considered to indicate a statistically significant difference.

Results

Features of cholesterol metabolism in LUAD identified by consensus clustering. Univariate Cox regression analysis was performed on 158 CMRGs, revealing that 44 of these genes were significantly associated with prognosis in LUAD (Table SI). Most of these 44 genes exhibited marked differential expression between LUAD and normal tissues (Fig. 1A). These 44 genes were further used to classify LUAD into two distinct cholesterol metabolism clusters based on their expression patterns (Fig. 1B). This clustering was validated by observing relative changes in the CDF curves (Fig. 1C) and the area under the curve (AUC) of CDF curves (Fig. 1D), with the optimal division (k=2) indicating the ideal number of clusters. When k=2, the delta area of CDF began to markedly decrease, thus choosing k=2 gave the best clustering effect (Fig. 1C and D). Survival analysis showed a significant difference in prognosis between the two clusters (Fig. 1E), with the Sankey diagram highlighting that cluster 1 contained more patients with lower Tumor-Node-Metastasis stages (23) and a better prognosis (Fig. 1F).

Potential functional pathways analysis. GSEA of Gene Ontology terms revealed that cluster 1 was primarily involved

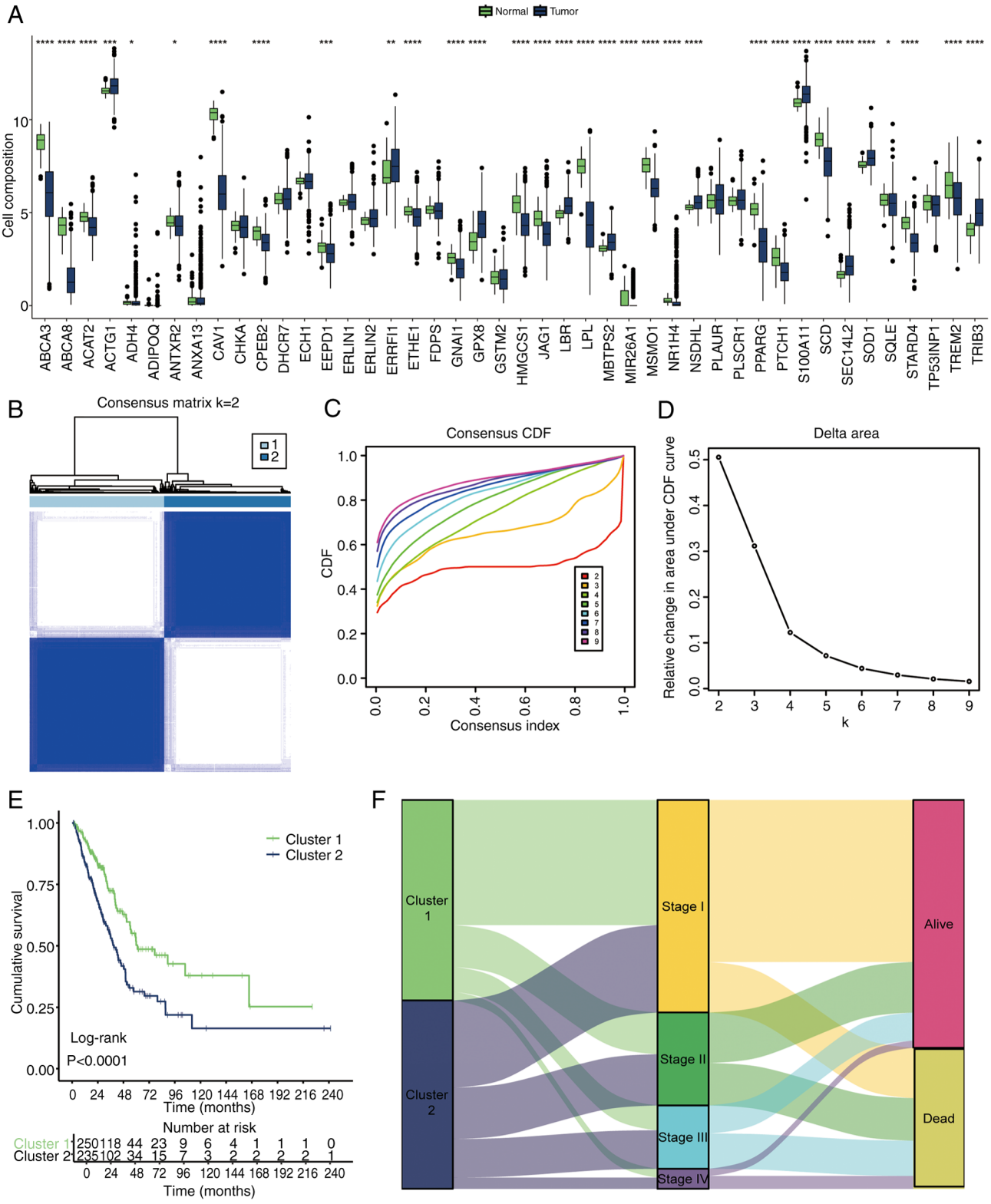

Figure 1. Consensus clustering identifying two LUAD subgroups with distinct cholesterol metabolism characteristics. (A) Differential expression of 44 prognostically relevant cholesterol metabolism-related genes in LUAD. (B) Consensus clustering matrix. (C) CDF curves for clusters. (D) Relative change in the area under the CDF curve. (E) Kaplan-Meier survival analysis. (F) Sankey diagram. *P<0.05, **P<0.01, ***P<0.001, ****P<0.0001. CDF, cumulative distribution function; LUAD, lung adenocarcinoma.

in 'POSITIVE REGULATION OF ENDOTHELIAL CELL DIFFERENTIATION', 'REGULATION OF CHOLESTEROL EFFLUX' and 'NEGATIVE REGULATION OF LIPID CATABOLIC PROCESS' (Fig. 2A). Given that enhanced cholesterol metabolism in tumors is associated with poor prognosis (24), these processes in cluster 1, which inhibit cholesterol metabolism and reduce the enrichment of cholesterol metabolites, were linked to a

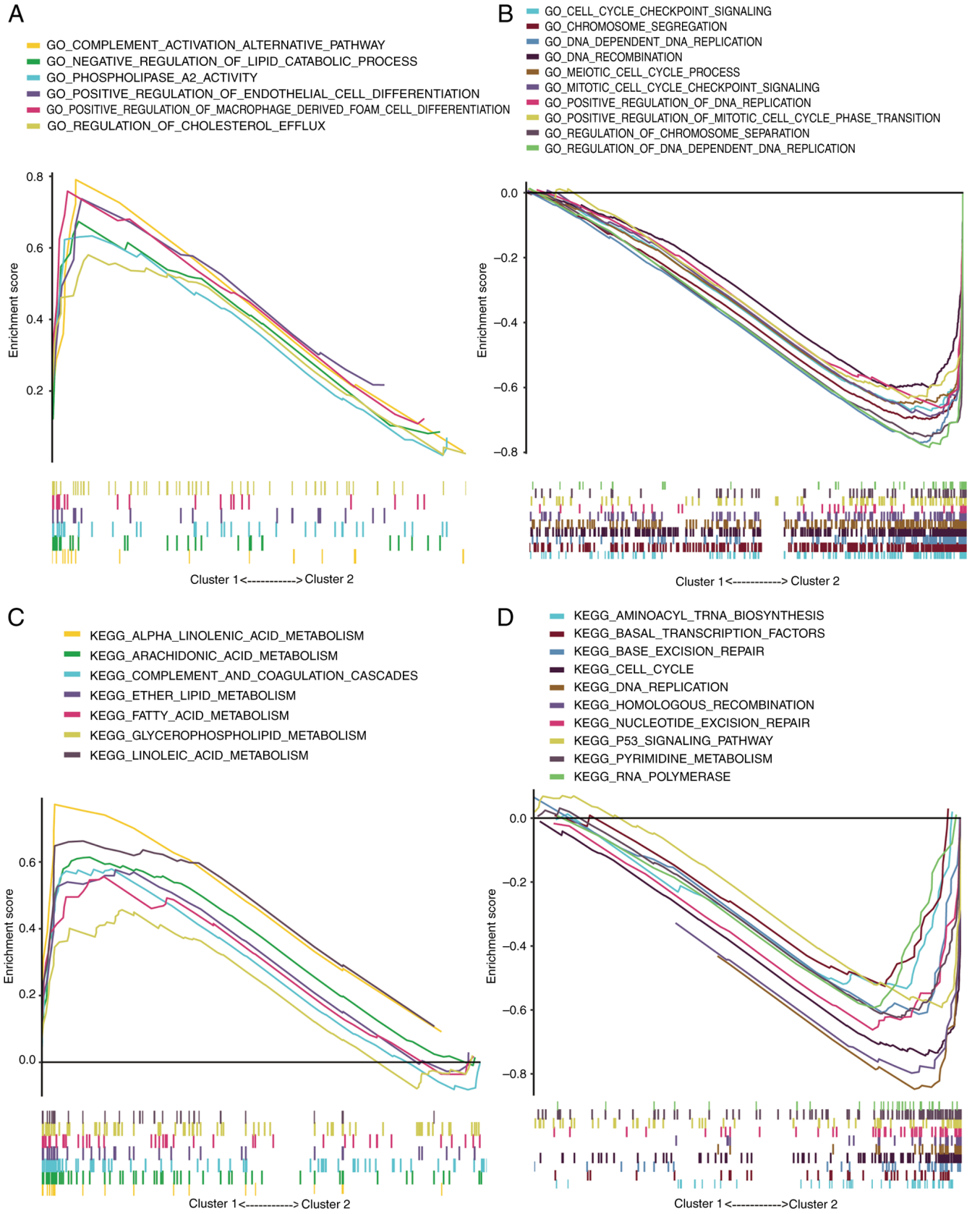

Figure 2. Gene set enrichment analysis revealing differences in pathways between the two cholesterol metabolism subgroups. GO enrichment in (A) cluster 1 and (B) cluster 2. KEGG enrichment in (C) cluster 1 and (D) cluster 2. GO, Gene Ontology; KEGG, Kyoto Encyclopedia of Genes and Genomes.

more favorable prognosis. Conversely, cluster 2 exhibited significant enrichment in processes such as 'CELL CYCLE CHECKPOINT SIGNALING', 'MEIOTIC CELL CYCLE PROCESS', 'MITOTIC CELL CYCLE CHECKPOINT SIGNALING', 'DNA DEPENDENT DNA REPLICATION' and 'DNA RECOMBINATION', contributing to accelerated

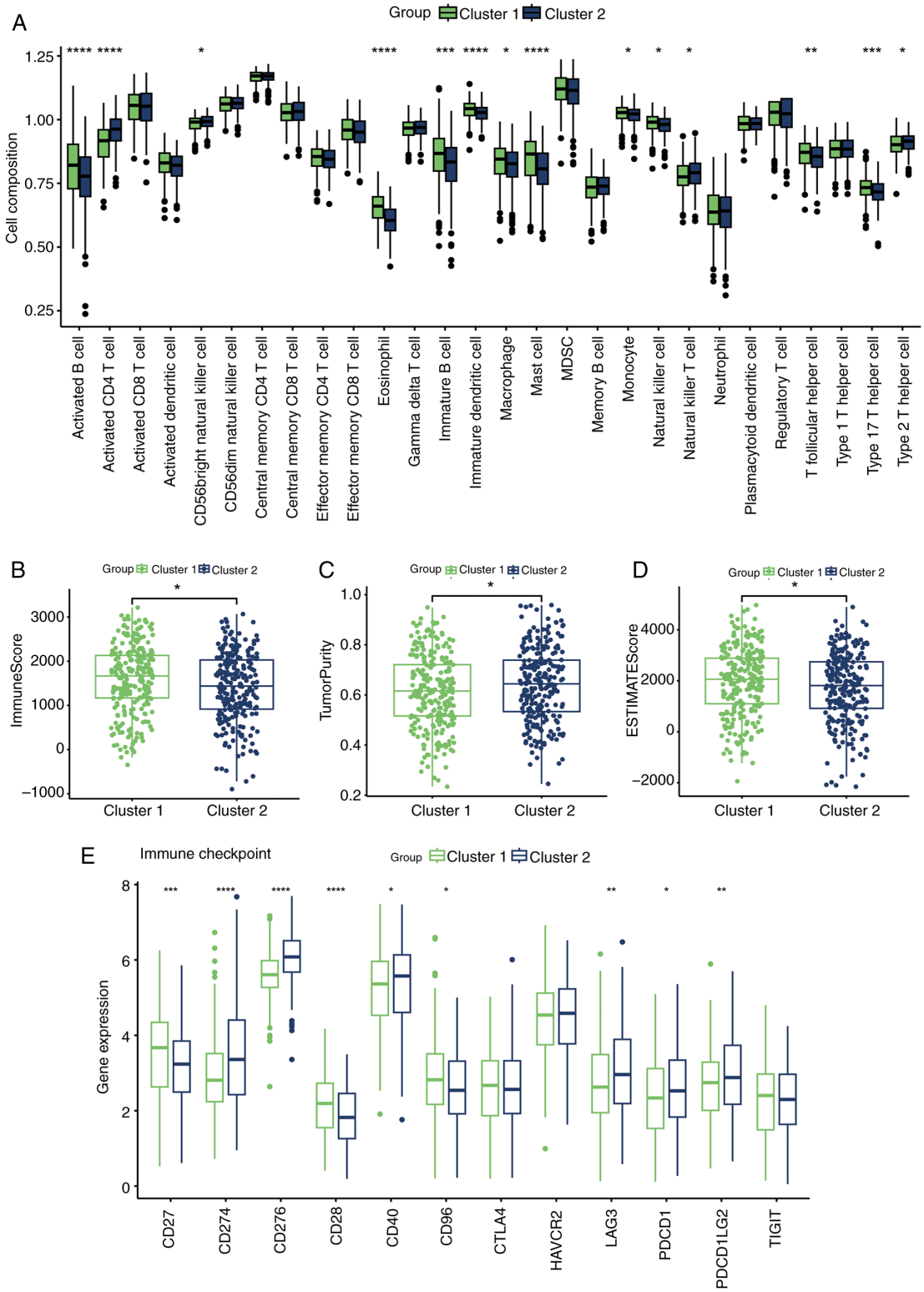

Figure 3. Tumor microenvironment assessment and prediction of immune cell infiltration. (A) Relative infiltration levels of 28 immune cells by single sample gene set enrichment analysis. Tumor microenvironment evaluation by ESTIMATE algorithm, including (B) immune score, (C) tumor purity and (D) ESTIMATE score. (E) Expression of key immune checkpoints in the two clusters. *P<0.05, **P<0.01, ***P<0.001, ****P<0.0001.

tumor progression (Fig. 2B). These findings were corroborated by Kyoto Encyclopedia of Genes and Genomes pathway analysis (Fig. 2C and D).

Immune infiltration analysis. Cholesterol metabolism reprogramming has been shown to be significantly associated with the formation of an immunosuppressive microenvironment (6). To investigate this further, the infiltration of 28 immune cell types was assessed across the clusters. Cluster 1, with a better prognosis, exhibited more abundant immune cell infiltration (Fig. 3A), with the majority of these cells having antitumor effects, such as B cells, macrophages, mast cells, natural killer cells, T follicular

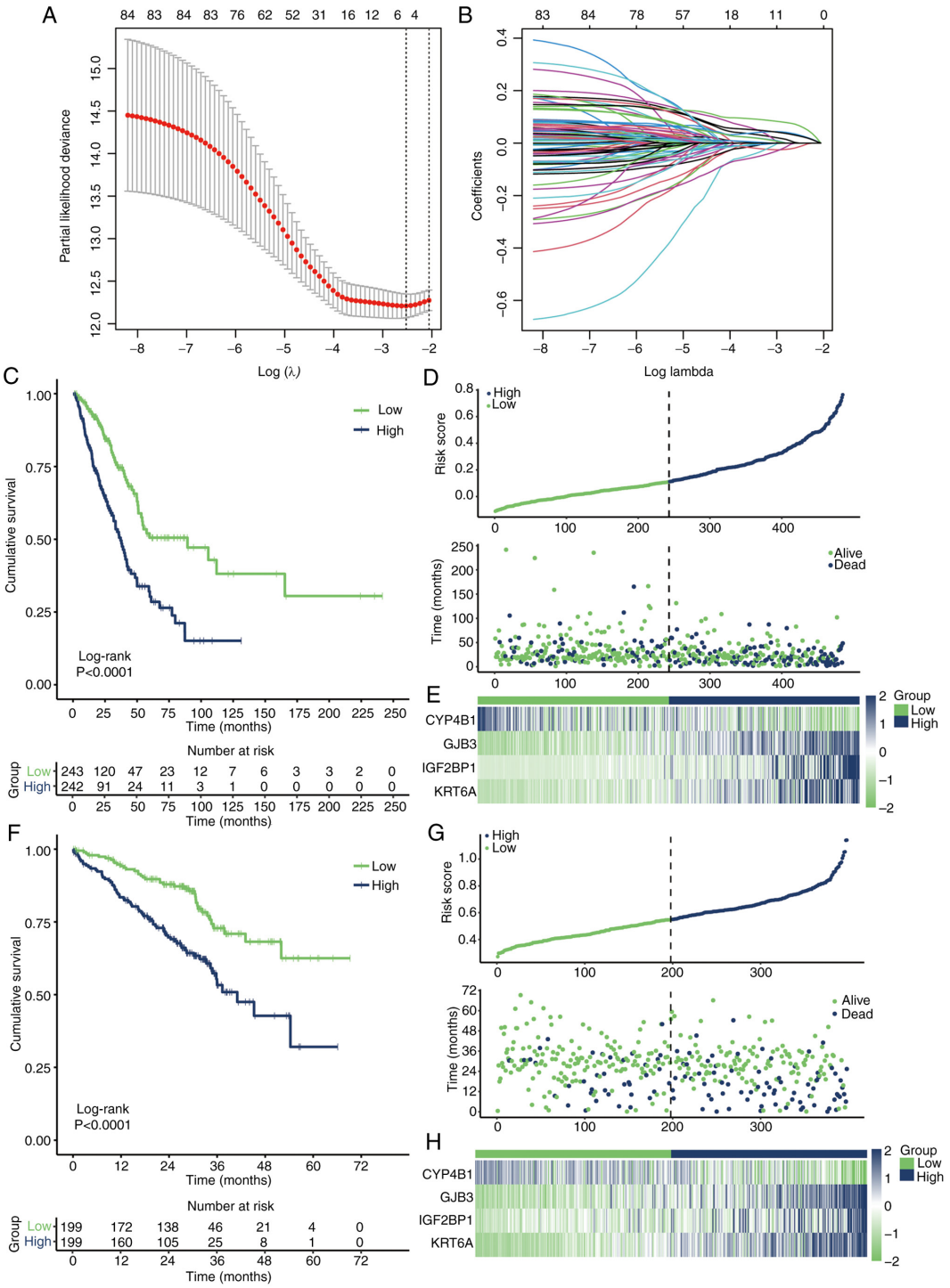

Figure 4. Construction and validation of the cholesterol metabolism gene signature. (A) LASSO Cox regression model for parameter (λ) adjustment through 10-fold cross-validation. (B) Identification of five key CMRGs and their corresponding coefficients. (C) KM survival analysis in TCGA dataset. (D) Relationship between mortality rates and risk scores in TCGA dataset. (E) Expression patterns of key CMRGs in TCGA dataset. (F) KM survival analysis in GSE72094. (G) Relationship between mortality rates and risk scores in GSE72094. (H) Expression patterns of key CMRGs in GSE72094. KM, Kaplan-Meier; TCGA, The Cancer Genome Atlas; CMRGs, cholesterol metabolism-related genes.

helper cells and type 17 T helper cells (25). Additionally, the ESTIMATE algorithm analysis confirmed the higher levels of immune cell infiltration in cluster 1 (Fig. 3B-D). Furthermore, the expression of immunosuppressive checkpoints is known to be associated with immunotherapy responses (26), and most immunosuppressive checkpoints commonly targeted in clinical practice were more closely associated with cluster 2, such as CD274, CD276, LAG3, PDCD1 and PDCD1LG2 (Fig. 3E).

Construction and validation of CMRG signature. Limma differential analysis identified 124 differentially expressed genes between cluster 1 and cluster 2. Univariate Cox regression identified 85 genes associated with prognosis (Table SII). Using the optimal λ value (Fig. 4A and B), four key genes: CYP4B1, GJB3, IGF2BP1 and KRT6A, were identified as significantly influencing the prognosis of the two clusters. The risk score for each patient was calculated using the following

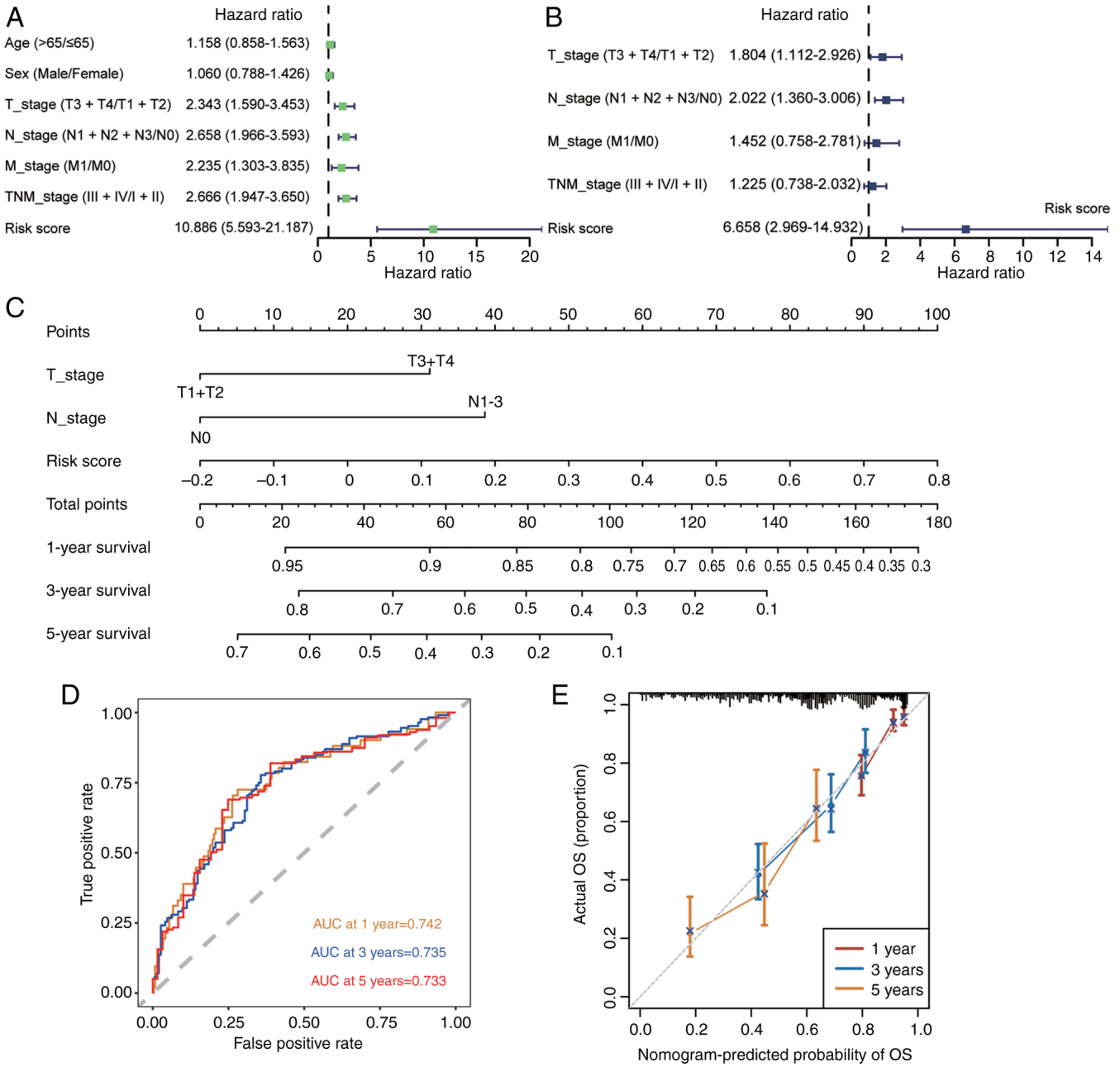

Figure 5. Application of the nomogram in the prognosis of LUAD. (A) Univariate and (B) multivariate Cox regression analyses to evaluate the association between CMRGs risk signals and LUAD prognosis. (C) Nomogram for quantifying the likelihood of patient survival. (D) Receiver operating characteristic curves of nomogram performance. (E) Calibration curves. AUC, area under the curve; LUAD, lung adenocarcinoma; CMRGs, cholesterol metabolism-related genes.

formula: Risk score=CYP4B1 x -0.01406345 + GJB3 x 0.03109533 + IGF2BP1 x 0.06671392 + KRT6A x 0.02723521. This model effectively distinguished patient prognoses in TCGA-LUAD cohort (Fig. 4C). The risk factor distribution graph demonstrated a higher mortality rate in the high-risk group (Fig. 4D), and the heatmap illustrated the distribution of the four key genes across different patients (Fig. 4E). Applying the same risk score formula to the GSE72094 dataset yielded similar results (Fig. 4F-H), further validating the effectiveness of the prognostic model.

Construction and validation of the nomogram. Univariate and multivariate Cox regression analyses of the key features affecting prognosis found that CMRG risk signature was an independent prognostic risk factor (Fig. 5A and B). Based on the CMRG risk signature and clinical characteristics, a nomogram prediction model was constructed (Fig. 5C). The AUC values for 1-, 3- and 5-year predictions were 0.742, 0.735 and 0.733, respectively (Fig. 5D). In addition, the prediction results of the nomogram closely aligned with the actual outcomes (Fig. 5E).

Analysis of TMB. Gene mutations are critical factors influencing tumor prognosis (27). TMB analysis of patients in different risk groups showed that most of the top 10 mutated genes overlapped between the two groups (Fig. 6A and B), but

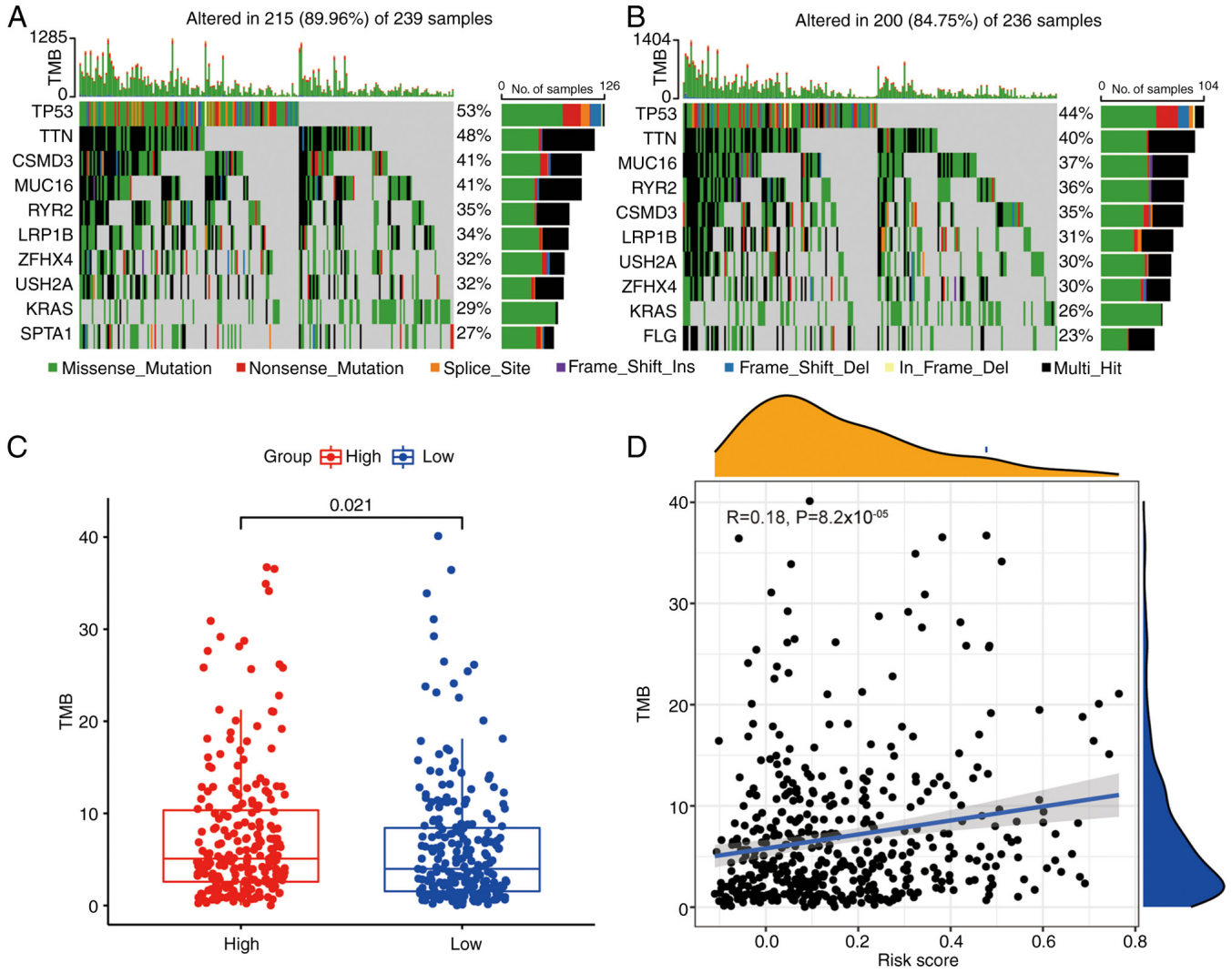

Figure 6. TMB analysis in the high-risk lung adenocarcinoma group. (A) Top 20 genes with mutation frequencies in the high-risk group. (B) Top 20 genes with mutation frequencies in the low-risk group. (C) Comparison of TMB between high-risk and low-risk groups. (D) Correlation analysis between risk score and TMB. TMB, tumor mutation burden.

mutation incidence was higher in the high-risk group (Fig. 6C). In addition, a low positive association was confirmed between risk score and TMB (Fig. 6D).

Prediction of immunotherapy and chemotherapy response. Using the TIDE algorithm, the potential effects of immunotherapy for patients with LUAD were successfully modeled and predicted. Notably, high-risk patients exhibited higher exclusion scores and TIDE values, while there was no significant difference in dysfunction scores (Fig. 7A), indicating a greater likelihood of drug resistance during immunotherapy compared with low-risk patients. Further analysis revealed that the percentage of low-risk patients responding positively to immunotherapy was significantly higher than that of high-risk patients (Fig. 7B), providing valuable insights for clinical decision-making. Additionally, the sensitivity of various chemotherapeutic agents within the patient cohort was assessed. Multiple chemotherapy drugs, such as cisplatin, docetaxel and doxorubicin, showed lower half-maximal inhibitory concentration values in the high-risk group, indicating that high-risk patients were more likely to benefit from these chemotherapy drugs (Fig. 7C), offering an expanded understanding of treatment options and providing a scientific foundation for personalized treatment strategies.

GJB3 promotes the proliferation, invasion and epithelial-mesenchymal transition (EMT) of LUAD. Bioinformatics analysis revealed that GJB3 was highly expressed in tumor tissues and functioned as an oncogene (Table SII). This was confirmed through *in vitro* validation. siRNA-mediated knockdown of GJB3 expression in A549 and NCI-H1975 cells (Fig. 8A and H) resulted in significantly reduced cell viability (Fig. 8B). In addition, EdU staining and colony formation assays showed that GJB3 knockdown decreased the proliferative capacity of both A549 and NCI-H1975 cells (Fig. 8C and D, and S1). Transwell assays further demonstrated that GJB3 knockdown inhibited the migration and invasion of these cells (Fig. 8E and F). Given that GJB3 encodes a key member of the connexin gene family (28), its alteration might impact EMT. Further examination revealed that GJB3 knockdown downregulated the expression levels

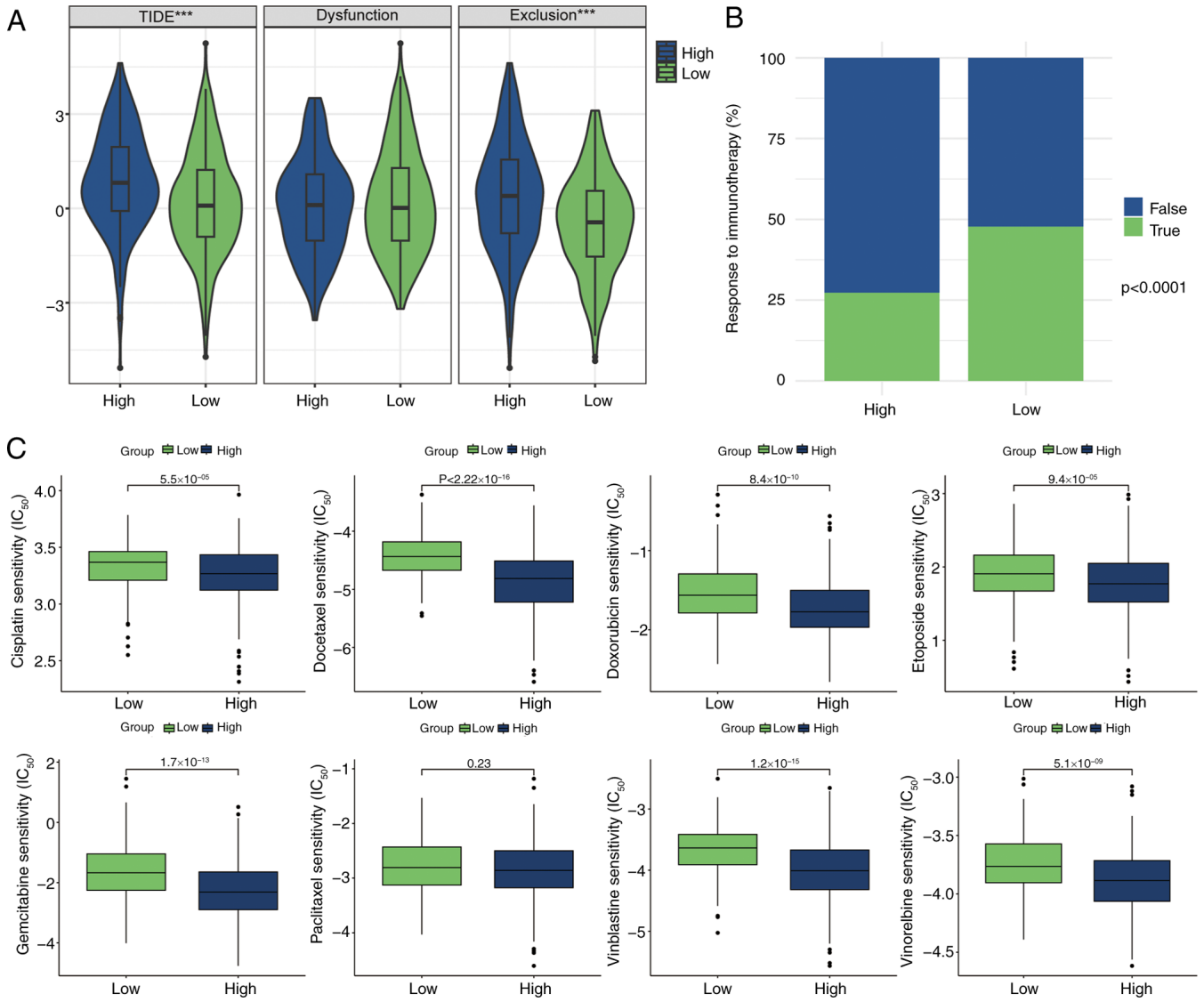

Figure 7. Treatment response prediction based on the cholesterol metabolism gene signature. (A) TIDE score comparison between the two risk groups. (B) Response rate comparison between the two risk groups. (C) Sensitivity of different risk groups to chemotherapy drugs. ***P<0.001. TIDE, Tumor Immune Dysfunction and Exclusion.

of vimentin, Snail1 and N-cadherin, while upregulating E-cadherin levels in A549 and NCI-H1975 cells (Fig. 8G), thus indicating that GJB3 knockdown inhibited the EMT process in these cell lines.

Discussion

The treatment of NSCLC faces notable challenges, including treatment resistance and the need for personalized therapies. Although traditional chemotherapy and radiotherapy remain essential components of NSCLC management, innovative treatment strategies have emerged in recent years (29). Immunotherapy, such as anti-PD-1/PD-L1 therapy, one of the most promising advancements, has demonstrated marked therapeutic effects and survival benefits by stimulating the immune system of patients to target and eliminate cancer cells (30). By contrast, targeted therapies, such as EGFR-tyrosine kinase inhibitors (TKIs), ALK-TKIs and entrectinib, offer more tailored treatment options by focusing on specific molecular markers on tumor cells, enabling precise intervention. By identifying and targeting these markers with specific drugs, targeted therapies enhance treatment efficacy, improve patient quality of life and minimize side effects (31-33). Furthermore, genomics-guided therapy represents a new frontier in personalized treatment for NSCLC. By analyzing the genetic profile of tumors, this approach provides deeper insights into the genetic characteristics, mutations and potential resistance mechanisms of the tumor, enabling the development of more precise and effective treatment strategies (34). The combination of immunotherapy and targeted therapies has further advanced NSCLC treatment, leveraging the synergistic effects of both approaches to improve therapeutic outcomes while minimizing adverse effects, thus offering patients greater survival benefits and a better overall treatment experience (35).

Cholesterol serves a pivotal role in maintaining cellular homeostasis (36). Due to the limited availability of nutrients

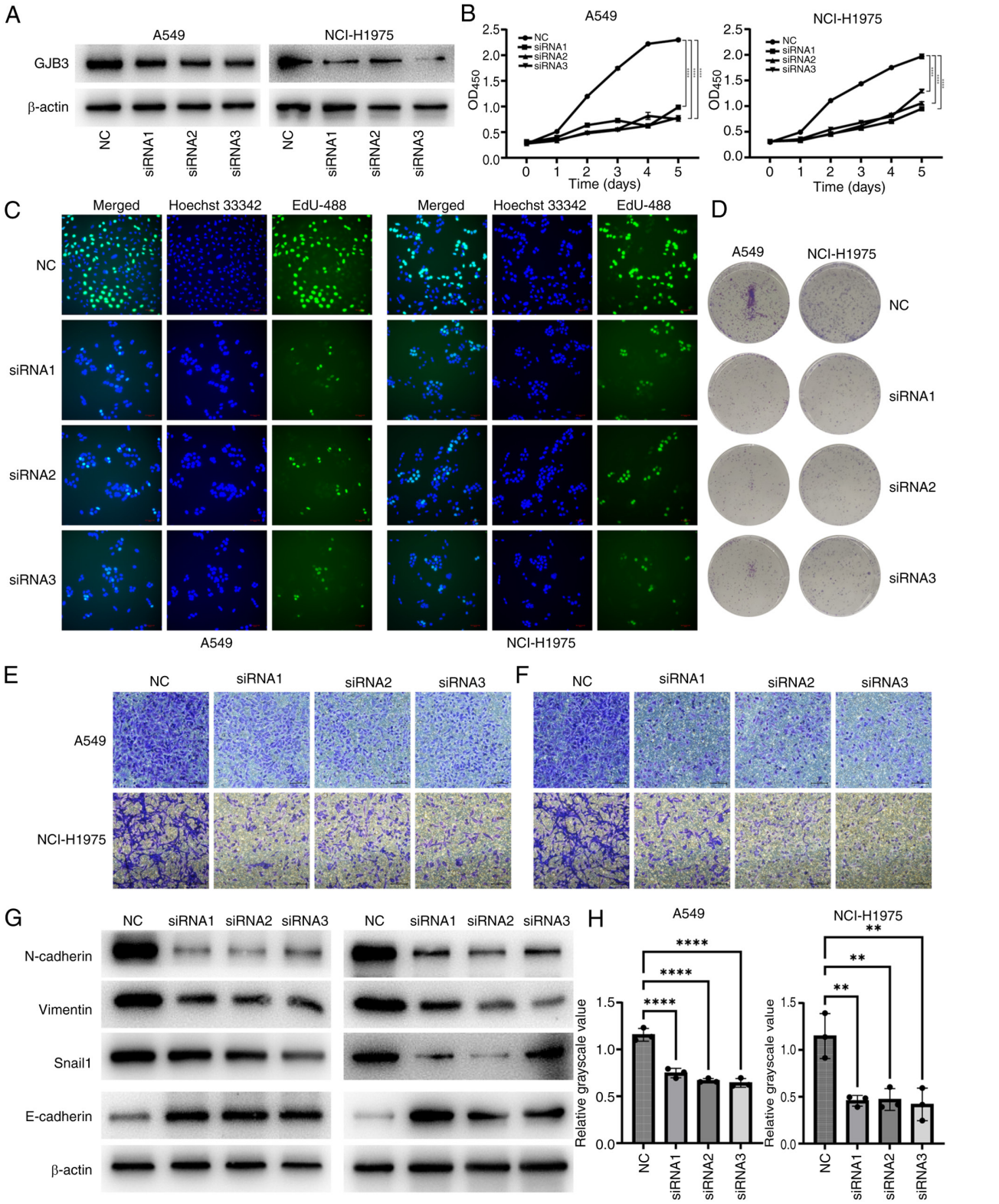

Figure 8. Effect of GJB3 expression on LUAD progression in *in vitro* experiments. (A) Knockdown efficiency of GJB3 after siRNA transfection, demonstrated by western blotting. (B) Knockdown of GJB3 enhanced LUAD cell proliferation. (C) EdU and (D) colony formation assays showed a decrease in the proportion of LUAD cells in the proliferative state after GJB3 knockdown (magnification, x200). (E) Migration and (F) invasion of LUAD cells was decreased after GJB3 knockdown (magnification, x200). (G) Knockdown of GJB3 inhibited the expression of epithelial-mesenchymal transition-related genes. (H) Semi-quantitative analysis of western blotting in (A). **P<0.01, ****P<0.0001. LUAD, lung adenocarcinoma; NC, negative control; siRNA, small interfering RNA.

in local tissues, tumors often experience relative nutrient deficiencies alongside the accumulation of metabolic waste products (37). In response to these adverse conditions, tumors undergo metabolic reprogramming to adapt (38). Preclinical studies have shown that inhibiting cholesterol synthesis can restrict tumor progression (39,40), and promising results have been reported from combining statins with other treatment modalities (41,42). Identifying key molecules involved in

cholesterol metabolism and developing targeted drugs against them are critical steps in advancing treatment for LUAD.

Cholesterol metabolism influences both tumor growth and the immune microenvironment (43), indicating a complex crosstalk between cholesterol metabolic status and the TME. Two distinct clusters with different cholesterol metabolism profiles were identified in the present study, with cluster 1 exhibiting richer immune cell infiltration, which helps explain the prognostic differences in patients with LUAD. Given the strong association between cholesterol metabolism and prognosis in LUAD, a prognostic model based on cholesterol metabolism was developed, involving CYP4B1, GJB3, IGF2BP1 and KRT6A. CYP4B1, a member of the cytochrome P450 enzyme superfamily, serves a key role in cholesterol and derivative synthesis. Its elevated expression in bladder cancer has been linked to an increased risk of the disease (44). IGF2BP1 influences tumor development and therapeutic responses primarily by binding to mRNAs, regulating their stability and translation (45). Müller *et al* (46) demonstrated that IGF2BP1 promotes SRF expression in an m6A-dependent manner, driving tumor growth and invasion. Additionally, Zhang *et al* (47) showed that IGF2BP1 overexpression accelerates the malignant progression of endometrial cancer through m6A methylation. Together, these studies highlight the importance of IGF2BP1 in understanding cancer progression. KRT6A is positively associated with both T-stage and N-stage in LUAD, and its knockdown inhibits cell proliferation, invasion and the EMT process in LUAD (48). Furthermore, GJB3 has been shown to be markedly upregulated in the liver metastases of pancreatic cancer, with overexpression enhancing the accumulation of tumor-associated neutrophils and promoting liver metastasis (49). The current study focused on GJB3, which is a member of the cell junction protein family. According to a previous report, high cholesterol metabolism can affect cell adhesion and promote tumor metastasis (50), and GJB3 may have an important role in this process. To further investigate its function, *in vitro* experiments were conducted, revealing that GJB3 knockdown inhibited the proliferative ability of LUAD cells, consistent with the results from GSEA. Additionally, GJB3 knockdown suppressed the migration and invasion of LUAD cells and reduced the expression of EMT-related proteins. These findings suggested that GJB3 may serve a critical role in LUAD progression and could serve as a potential therapeutic target.

Cholesterol metabolism influences the TME and may significantly affect the efficacy of immunotherapy (51). The CMRG score constructed in the current study suggested that low-risk patients exhibited higher response rates to immune checkpoint therapy, whereas high-risk patients were predicted to show a better chemotherapy response. This highlights new perspectives for the precision treatment of patients with LUAD.

There are some limitations in the present study: The sequencing data comes from previous patients, and the characteristics of cholesterol metabolism were only studied in TCGA and GSE72094 datasets. It is necessary to conduct larger prospective studies to further confirm the effectiveness of the prognostic model. Second, the cancer-promoting ability of GJB3 in LUAD needs further validation in animals. Notably, the mechanism by which GJB3 promotes the progression of LUAD by affecting cholesterol metabolism needs to be further studied through multi-omics, and *in vitro* and *in vivo* experiments.

In conclusion, cholesterol metabolic status is closely associated with the prognosis, TME and treatment response in patients with LUAD. The cholesterol metabolism-related prognostic model developed in the current study may not only predict patient outcomes but could also provide valuable insights into personalized treatment strategies.

Acknowledgements

Not applicable.

Funding

The present study was supported by the Natural Science Foundation of Guangdong Province (grant no. 2019A1515011601).

Availability of data and materials

The data generated in the present study may be requested from the corresponding author.

Authors' contributions

QY, WC and JW designed and supervised the experiments. WC and WW performed the bioinformatics analysis. LG and DL performed the experiments. QY and JY analyzed and interpreted the data, and wrote the first draft of the manuscript. QY, JW and WC reviewed the manuscript. LG and WC confirm the authenticity of all the raw data. All authors read and approved the final manuscript.

Ethics approval and consent to participate

Not applicable.

Patient consent for publication

Not applicable.

Competing interests

The authors declare that they have no competing interests.

References

1. Siegel RL, Miller KD and Jemal A: Cancer statistics, 2020. CA Cancer J Clin 70: 7-30, 2020.
2. Berg CD, Schiller JH, Boffetta P, Cai J, Connolly C, Kerpel-Fronius A, Kitts AB, Lam DCL, Mohan A, Myers R, *et al*: Air pollution and lung cancer: A review by international association for the study of lung cancer early detection and screening committee. J Thorac Oncol 18: 1277-1289, 2023.
3. Akçay S: Deciphering molecular overlaps between COPD and NSCLC subtypes (LUAD and LUSC): An integrative bioinformatics study. Medicine (Baltimore) 104: e43906, 2025.
4. Thai AA, Solomon BJ, Sequist LV, Gainor JF and Heist RS: Lung cancer. Lancet 398: 535-554, 2021.
5. Mamdani H, Matosevic S, Khalid AB, Durm G and Jalal SI: Immunotherapy in lung cancer: Current landscape and future directions. Front Immunol 13: 823618, 2022.

6. Huang B, Song BL and Xu C: Cholesterol metabolism in cancer: Mechanisms and therapeutic opportunities. Nat Metab 2: 132-141, 2020.
7. Bakiri L, Hamacher R, Graña O, Guío-Carrión A, Campos-Olivas R, Martinez L, Dienes HP, Thomsen MK, Hasenfuss SC and Wagner EF: Liver carcinogenesis by FOS-dependent inflammation and cholesterol dysregulation. J Exp Med 214: 1387-1409, 2017.
8. Wang X, Huang Z, Wu Q, Prager BC, Mack SC, Yang K, Kim LJY, Gimple RC, Shi Y, Lai S, *et al*: MYC-regulated mevalonate metabolism maintains brain tumor-initiating cells. Cancer Res 77: 4947-4960, 2017.
9. Kondo A, Yamamoto S, Nakaki R, Shimamura T, Hamakubo T, Sakai J, Kodama T, Yoshida T, Aburatani H and Osawa T: Extracellular acidic pH activates the sterol regulatory element-binding protein 2 to promote tumor progression. Cell Rep 18: 2228-2242, 2017.
10. He M, Zhang W, Dong Y, Wang L, Fang T, Tang W, Lv B, Chen G, Yang B, Huang P and Xia J: Pro-inflammation NF-κB signaling triggers a positive feedback via enhancing cholesterol accumulation in liver cancer cells. J Exp Clin Cancer Res 36: 15, 2017.
11. Kloudova A, Guengerich FP and Soucek P: The role of oxysterols in human cancer. Trends Endocrinol Metab 28: 485-496, 2017.
12. Raccosta L, Fontana R, Maggioni D, Lanterna C, Villablanca EJ, Paniccia A, Musumeci A, Chiricozzi E, Trincavelli ML, Daniele S, *et al*: The oxysterol-CXCR2 axis plays a key role in the recruitment of tumor-promoting neutrophils. J Exp Med 210: 1711-1728, 2013.
13. Goossens P, Rodriguez-Vita J, Etzerodt A, Masse M, Rastoin O, Gouirand V, Ulas T, Papantonopoulou O, Van Eck M, Auphan-Anezin N, *et al*: Membrane cholesterol efflux drives tumor-associated macrophage reprogramming and tumor progression. Cell Metab 29: 1376-1389.e4, 2019.
14. Kopecka J, Trouillas P, Gašparović AČ, Gazzano E, Assaraf YG and Riganti C: Phospholipids and cholesterol: Inducers of cancer multidrug resistance and therapeutic targets. Drug Resist Updat 49: 100670, 2020.
15. Schabath MB, Welsh EA, Fulp WJ, Chen L, Teer JK, Thompson ZJ, Engel BE, Xie M, Berglund AE, Creelan BC, *et al*: Differential association of STK11 and TP53 with KRAS mutation-associated gene expression, proliferation and immune surveillance in lung adenocarcinoma. Oncogene 35: 3209-3216, 2016.
16. Castanza AS, Recla JM, Eby D, Thorvaldsdottir H, Bult CJ and Mesirov JP: Extending support for mouse data in the molecular signatures database (MSigDB). Nat Methods 20: 1619-1620, 2023.
17. Wilkerson MD and Hayes DN: ConsensusClusterPlus: A class discovery tool with confidence assessments and item tracking. Bioinformatics 26: 1572-1573, 2010.
18. Subramanian A, Tamayo P, Mootha VK, Mukherjee S, Ebert BL, Gillette MA, Paulovich A, Pomeroy SL, Golub TR, Lander ES and Mesirov JP: Gene set enrichment analysis: A knowledge-based approach for interpreting genome-wide expression profiles. Proc Natl Acad Sci USA 102: 15545-15550, 2005.
19. Barbie DA, Tamayo P, Boehm JS, Kim SY, Moody SE, Dunn IF, Schinzel AC, Sandy P, Meylan E, Scholl C, *et al*: Systematic RNA interference reveals that oncogenic KRAS-driven cancers require TBK1. Nature 462: 108-112, 2009.
20. Yoshihara K, Shahmoradgoli M, Martinez E, Vegesna R, Kim H, Torres-Garcia W, Treviño V, Shen H, Laird PW, Levine DA, *et al*: Inferring tumour purity and stromal and immune cell admixture from expression data. Nat Commun 4: 2612, 2013.
21. Ritchie ME, Phipson B, Wu D, Hu Y, Law CW, Shi W and Smyth GK: limma powers differential expression analyses for RNA-sequencing and microarray studies. Nucleic Acids Res 43: e47, 2015.
22. Jiang P, Gu S, Pan D, Fu J, Sahu A, Hu X, Li Z, Traugh N, Bu X, Li B, *et al*: Signatures of T cell dysfunction and exclusion predict cancer immunotherapy response. Nat Med 24: 1550-1558, 2018.
23. Rami-Porta R, Nishimura KK, Giroux DJ, Detterbeck F, Cardillo G, Edwards JG, Fong KM, Giuliani M, Huang J, Kernstine KH Sr, *et al*: The international association for the study of lung cancer lung cancer staging project: Proposals for revision of the TNM stage groups in the forthcoming (ninth) edition of the TNM classification for lung cancer. J Thorac Oncol 19: 1007-1027, 2024.
24. Ehmsen S, Pedersen MH, Wang G, Terp MG, Arslanagic A, Hood BL, Conrads TP, Leth-Larsen R and Ditzel HJ: Increased cholesterol biosynthesis is a key characteristic of breast cancer stem cells influencing patient outcome. Cell Rep 27: 3927-3938.e6, 2019.
25. Turley SJ, Cremasco V and Astarita JL: Immunological hallmarks of stromal cells in the tumour microenvironment. Nat Rev Immunol 15: 669-682, 2015.
26. Zhang Y and Zhang Z: The history and advances in cancer immunotherapy: Understanding the characteristics of tumor-infiltrating immune cells and their therapeutic implications. Cell Mol Immunol 17: 807-821, 2020.
27. Martínez-Jiménez F, Muiños F, Sentís I, Deu-Pons J, Reyes-Salazar I, Arnedo-Pac C, Mularoni L, Pich O, Bonet J, Kranas H, *et al*: A compendium of mutational cancer driver genes. Nat Rev Cancer 20: 555-572, 2020.
28. Liu J, Wang X, Jiang W, Azoitei A, Eiseler T, Eckstein M, Hartmann A, Stilgenbauer S, Elati M, Hohwieler M, *et al*: Impairment of α-tubulin and F-actin interactions of GJB3 induces aneuploidy in urothelial cells and promotes bladder cancer cell invasion. Cell Mol Biol Lett 29: 94, 2024.
29. Otano I, Ucero AC, Zugazagoitia J and Paz-Ares L: At the crossroads of immunotherapy for oncogene-addicted subsets of NSCLC. Nat Rev Clin Oncol 20: 143-159, 2023.
30. Sui H, Ma N, Wang Y, Li H, Liu X, Su Y and Yang J: Anti-PD-1/PD-L1 therapy for non-small-cell lung cancer: Toward personalized medicine and combination strategies. J Immunol Res 2018: 6984948, 2018.
31. Santoni-Rugiu E, Melchior LC, Urbanska EM, Jakobsen JN, Stricker K, Grauslund M and Sørensen JB: Intrinsic resistance to EGFR-tyrosine kinase inhibitors in EGFR-mutant non-small cell lung cancer: Differences and similarities with acquired resistance. Cancers (Basel) 11: 923, 2019.
32. Shaw AT, Solomon BJ, Besse B, Bauer TM, Lin CC, Soo RA, Riely GJ, Ou SI, Clancy JS, Li S, *et al*: ALK Resistance mutations and efficacy of lorlatinib in advanced anaplastic lymphoma kinase-positive non-small-cell lung cancer. J Clin Oncol 37: 1370-1379, 2019.
33. Drilon A, Siena S, Dziadziuszko R, Barlesi F, Krebs MG, Shaw AT, de Braud F, Rolfo C, Ahn MJ, Wolf J, *et al*: Entrectinib in ROS1 fusion-positive non-small-cell lung cancer: Integrated analysis of three phase 1-2 trials. Lancet Oncol 21: 261-270, 2020.
34. Wang Z, Zhang Q, Qi C, Bai Y, Zhao F, Chen H, Li Z, Wang X, Chen M, Gong J, *et al*: Combination of AKT1 and CDH1 mutations predicts primary resistance to immunotherapy in dMMR/MSI-H gastrointestinal cancer. J Immunother Cancer 10: e004703, 2022.
35. Wang M, Herbst RS and Boshoff C: Toward personalized treatment approaches for non-small-cell lung cancer. Nat Med 27: 1345-1356, 2021.
36. King RJ, Singh PK and Mehla K: The cholesterol pathway: Impact on immunity and cancer. Trends Immunol 43: 78-92, 2022.
37. Pavlova NN, Zhu J and Thompson CB: The hallmarks of cancer metabolism: Still emerging. Cell Metab 34: 355-377, 2022.
38. Hanahan D: Hallmarks of cancer: New dimensions. Cancer Discov 12: 31-46, 2022.
39. Li J, Liu J, Liang Z, He F, Yang L, Li P, Jiang Y, Wang B, Zhou C, Wang Y, *et al*: Simvastatin and Atorvastatin inhibit DNA replication licensing factor MCM7 and effectively suppress RB-deficient tumors growth. Cell Death Dis 8: e2673, 2017.
40. Mullen PJ, Yu R, Longo J, Archer MC and Penn LZ: The interplay between cell signalling and the mevalonate pathway in cancer. Nat Rev Cancer 16: 718-731, 2016.
41. Lee J, Jung KH, Park YS, Ahn JB, Shin SJ, Im SA, Oh DY, Shin DB, Kim TW, Lee N, *et al*: Simvastatin plus irinotecan, 5-fluorouracil, and leucovorin (FOLFIRI) as first-line chemotherapy in metastatic colorectal patients: A multicenter phase II study. Cancer Chemother Pharmacol 64: 657-663, 2009.
42. Liu JC, Hao WR, Hsu YP, Sung LC, Kao PF, Lin CF, Wu AT, Yuan KS and Wu SY: Statins dose-dependently exert a significant chemopreventive effect on colon cancer in patients with chronic obstructive pulmonary disease: A population-based cohort study. Oncotarget 7: 65270-65283, 2016.
43. Liu X, Lv M, Zhang W and Zhan Q: Dysregulation of cholesterol metabolism in cancer progression. Oncogene 42: 3289-3302, 2023.
44. Imaoka S, Yoneda Y, Sugimoto T, Hiroi T, Yamamoto K, Nakatani T and Funae Y: CYP4B1 is a possible risk factor for bladder cancer in humans. Biochem Biophys Res Commun 277: 776-780, 2000.
45. Wang T, Kong S, Tao M and Ju S: The potential role of RNA N6-methyladenosine in cancer progression. Mol Cancer 19: 88, 2020.

46. Müller S, Glaß M, Singh AK, Haase J, Bley N, Fuchs T, Lederer M, Dahl A, Huang H, Chen J, *et al*: IGF2BP1 promotes SRF-dependent transcription in cancer in a m6A- and miRNA-dependent manner. Nucleic Acids Res 47: 375-390, 2019.
47. Zhang L, Wan Y, Zhang Z, Jiang Y, Gu Z, Ma X, Nie S, Yang J, Lang J, Cheng W and Zhu L: IGF2BP1 overexpression stabilizes PEG10 mRNA in an m6A-dependent manner and promotes endometrial cancer progression. Theranostics 11: 1100-1114, 2021.
48. Yang B, Zhang W, Zhang M, Wang X, Peng S and Zhang R: KRT6A promotes EMT and cancer stem cell transformation in lung adenocarcinoma. Technol Cancer Res Treat 19: 1533033820921248, 2020.
49. Huo Y, Zhou Y, Zheng J, Jin G, Tao L, Yao H, Zhang J, Sun Y, Liu Y and Hu LP: GJB3 promotes pancreatic cancer liver metastasis by enhancing the polarization and survival of neutrophil. Front Immunol 13: 983116, 2022.
50. Mohammadalipour A, Showalter CA, Muturi HT, Farnoud AM, Najjar SM and Burdick MM: Cholesterol depletion decreases adhesion of non-small cell lung cancer cells to E-selectin. Am J Physiol Cell Physiol 325: C471-C482, 2023.
51. Ngwa VM, Edwards DN, Philip M and Chen J: Microenvironmental metabolism regulates antitumor immunity. Cancer Res 79: 4003-4008, 2019.

Copyright © 2025 Yan et al. This work is licensed under a Creative Commons Attribution-NonCommercial-NoDerivatives 4.0 International (CC BY-NC-ND 4.0) License.